Desalination and Water Treatment
www.deswater.com

doi: 10.5004/dwt.2020.25588

190 (2020) 294–311
June

Removal of orange II from aqueous solutions using micro-mesoporous carbon materials: kinetic and equilibrium studies

Katarzyna Jedynak*, Marta Repelewicz, Krystyna Kurdziel, Dariusz Wideł

Institute of Chemistry, Jan Kochanowski University, Świętokrzyska 15G, 25-406 Kielce, Poland, emails: kjedynak@ujk.edu.pl (K. Jedynak), martar@ujk.edu.pl (M. Repelewicz), krystyna.kurdziel@ujk.edu.pl (K. Kurdziel), dwidel@ujk.edu.pl (D. Wideł)

Received 22 September 2019; Accepted 27 January 2020

ABSTRACT

Adsorption of orange II from aqueous solutions on two carbon materials (ST-A and ST-A-CO_2) obtained by the soft-templating method and commercial activated carbon (CWZ 22) was studied. The surface properties of carbons were characterized by nitrogen adsorption isotherms and scanning electron microscopy, the Boehm's titration method and the point of zero charge (pH_{PZC}). Investigated adsorbents have specific surface areas from 710 to 950 $m^2 g^{-1}$. Adsorption isotherms, adsorption kinetics, the effect of pH solution (2–10) and temperature (298°K, 308°K, and 315°K) on adsorption of orange II on the carbon materials were studied. The experimental data has been described by Langmuir, Langmuir–Freundlich, Freundlich, and Dubinin–Radushkevich adsorption isotherm models. The Langmuir model is the best to describe the received experimental data. Results of adsorption experiments showed that the studied carbons exhibited high adsorption capacity in relation to orange II. The highest adsorption capacity was obtained for carbon ST-A-CO_2 (322 mg g^{-1}). Maximum adsorption for adsorbents ST-A and CWZ-22 were 127 and 206 mg g^{-1}, respectively. To explain the kinetic model of adsorption, the pseudo-first-order kinetic model, the pseudo-second-order kinetic model, and the intra-particle diffusion model were used. Adsorption of orange II on all studied carbons runs according to the pseudo-second-order model. The calculated thermodynamic function indicated that the adsorption processes of orange II on all carbon materials were spontaneous and endothermic (ΔH is 22.58, 18.21, and 23.67 kJ mol^{-1} for ST-A, ST-A-CO_2, and CWZ, respectively).

Keywords: Adsorption; Orange II; Micro-mesoporous carbons; Functional groups; pH_{PZC}; Effect of pH solution; Effect of temperature; Isotherm; Kinetic; Thermodynamic

1. Introduction

One of the most serious environmental pollutants are dyes. Their use in excess causes hazards to human health. Many of them are considered to be toxic, mutagenic, and even carcinogenic [1–3]. Dyes are harmful to the ecosystems present in water reservoirs, undergo various chemical and biological transformations, they can prevent photosynthesis by absorbing sunlight. Dyes containing sulfur in their structure can quickly reduce oxygen in the water and consume it [4,5]. Orange II (OII) [6,7], also known as Acid Orange 7 [8,9] belongs to the anionic dyes from the azo group [10]. Due to the fact that this dye is commonly used in the industry mainly paper and textile, large quantities of it get into the water with sewage, which is why it is very important to remove OII from water. Orange II is a highly toxic dye, and its intake may cause irritation to eyes, skin, mucous membranes, and upper respiratory tracts, moreover, it may cause severe headaches and nausea [4].

Environmental wastewater produced in this way should be removed before it reaches water reservoirs [11]. Problems associated with dye contamination can be reduced or minimized by various chemical, biological, and physical processes. However, these processes have their limitations and drawbacks, such as high costs, poor removal efficiency, secondary pollution generation, and others. The adsorption

---

* Corresponding author.

process was considered the most suitable for removing dyes from aqueous solutions due to its efficiency and economy [12]. It is important to find adsorbents that in a very short time and high yield will adsorb dyes from the water environment [13,14].

Such adsorbents can be porous carbon materials, including mesoporous carbon materials because they are characterized by high thermal stability, resistance to acids and bases, and biocompatibility [15,16]. They have found a special application in the adsorption of dyes and purification of water from organic impurities because of the well-developed specific surface area (S_{BET}), and pore volume [17].

There are two main methods for the synthesis of ordered mesoporous carbons. The first of these is the method of hard-templating using ordered mesoporous silicas, silica colloids, or colloidal silica crystals. The second one is a soft-templating method, which uses surface-active compounds (surfactants) or blocks copolymers as soft matrixes [18–22]. The soft-templating method is in contrast to the hard-templating method, eliminates the necessity of using solid silica matrices, which consequently reduced the number of synthesis steps and made the process cheaper and easier to implement from the industrial point of view [23–28].

In many applications, it is required that mesoporous materials, in addition to large and homogeneous mesopores, should also contain micropores having high adsorptive capacity. The hard and soft-templating methods allow to develop the good mesoporosity, while the obtained carbon materials are characterized by very poor development of microporosity. Therefore, to increase the range of applications of mesoporous carbons, their physical (e.g., activation by CO_2) or chemical (e.g., activation with KOH) modifications are performed [29].

The aim of the work was to compare the adsorption properties of two synthesized carbons and one commercial carbon for adsorption of orange II from aqueous solutions. The nitrogen adsorption isotherms and scanning electron microscopy (SEM), were used to characterize the surface properties of adsorbents. Additionally, the surface functional acidic and basic groups were determined using Boehm's method. Factors affecting the adsorption process such as the effect of contact time, pH, and initial dye concentration were analyzed. The Langmuir, Freundlich, Langmuir–Freundlich, and Dubinin–Radushkevich adsorption isotherm models, were applied to analyze the experimental data. Selected kinetic models (pseudo-first-order, pseudo-second-order, and intraparticle diffusion model) for the adsorption of dye were also presented. In order to better understand the nature of the adsorption process, thermodynamic functions were determined. The interaction mechanism between OII and studied carbons was proposed to analyze the obtained results.

2. Materials and methods

2.1. Reagents

The used adsorbent is anionic (azo) dye—orange II sodium salt ($C_{16}H_{11}N_2NaO_4S$, M_{mol} = 350.32 g mol^{-1}) from Sigma-Aldrich (Germany). The chemical structure of the dye is shown in Fig. 1. The maximum absorbance of the dye is at a wavelength of 485 nm.

The mesoporous carbon (ST-A) obtained by the soft templating method and the micro-mesoporous carbon (ST-A-CO_2) obtained analogously to ST-A and then activated with CO_2, were used as the adsorbents. In order to compare the adsorption properties of commercial carbon (CWZ-22; GRYFSKAND, Hajnowka, Poland) was used.

2.2. Preparation of adsorbents

Mesoporous carbons were prepared by the soft-templating method according to a slightly modified recipe of Wang et al. [30] and similar to that reported in the work of Choma et al. [31]. During the synthesis, Pluronic F127 was used and the amount of all reagents were three times greater than in the work. In a typical synthesis, 7.5 g of resorcinol and 7.5 g of Pluronic F127 triblock copolymer were dissolved in 35.7 cm^3 of ethanol and 19.8 cm^3 of water. After complete dissolution, the reaction mixture was supplied with 2.2 cm^3 of 37% hydrochloric acid as a catalyst and stirred for an additional 30 min. Next, 7.5 cm^3 of 37% formaldehyde was added into the synthesis mixture and stirred until turned cloudy and allowed to separate into two layers. The polymer-rich bottom layer was spread onto quartz boats and heated in a furnace at 373 K for 24 h. Thermal treatment and carbonization of the resulting film were performed in the tube furnace under nitrogen flow using temperature program: 1 K min^{-1} up to 673 K, then 5 K min^{-1} up to 1,123 K, and held for 2 h. The obtained material was marked as ST-A.

Obtained ST-A material was activated by CO_2, according to a slightly modified recipe of Wickramaratne and Jaroniec [32]. The post-synthesis activation of mesoporous carbon was performed by placing a quartz boat with 3 g of ST-A in a ceramic tube furnace under flowing nitrogen with a heating rate of 10 K min^{-1} up to 1,123 K. After reaching this temperature, the activating gas was introduced to the tube furnace (50 cm^3 min^{-1}) for 8 h and then switched back to nitrogen to prevent further activation during the cooling process. The obtained activated materials are denoted as ST-A-CO_2. After the synthesis, both carbons were washed with distilled water to pH = 7 and dried to a constant mass.

2.3. Characterization of adsorbents

2.3.1. Porous structure of adsorbents

The porous structure of applied adsorbents was designated on the basis of low-temperature nitrogen adsorption isotherms (77 K), using a volumetric adsorption analyzer ASAP 2020 by Micromeritics (Norcross, GA, USA; Structural

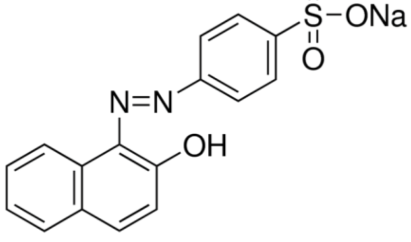

Fig. 1. Chemical formula of OII.

Research Laboratory of Jan Kochanowski University in Kielce). Before adsorptive measurements, all the carbon samples were degassed in temp. 473 K for 2 h. Experimental nitrogen adsorption isotherms were used to determine the standard parameters of the porous structure such as S_{BET}, pore volume, and pore size distribution. The S_{BET} was determined in the relative pressure range from 0.05 to 0.20 considering the surface (0.162 nm^2) occupied by a single nitrogen molecule in a monolayer [33]. The total pore volume (V_t) was determined from one point of the adsorption isotherm corresponding to the relative pressure p/p_0 = 0.99 [34]. The pore size distribution functions were calculated by using the non-local density functional theory method for carbon slit-shaped pores with surface energetical heterogeneity and geometrical corrugation [35,36]. The calculations were performed using the numerical program SAIEUS (Micromeritics, USA).

Photos of investigated carbon materials were obtained by SEM Zeiss mod. Ultra Plus, energy dispersive spectroscopy (EDS) Bruker Quantax 400. During the measurements, a voltage of 2 kV was applied.

The functional acidic and basic groups containing oxygen on the surface of studied carbon materials were determined using Boehm's titration method [37,38]. Mass 0.2 g of obtained carbon materials were dispersed in the following solution: sodium bicarbonate, sodium carbonate, sodium hydroxide, sodium ethoxide to determine functional acidic groups, and hydrochloric acid to determine total basic groups. Then the solution was shaken for 48 h at room temperature (Table 1). The sample was then filtered and 10 cm^3 of the filtrate was titrated with 0.1 mol dm^{-3} HCl to determine acidic groups and 0.05 mol dm^{-3} NaOH to determine total basic groups.

The point of zero charge (pH_{PZC}) of studied carbon was analyzed according to the method proposed in works [39,40]. At first 0.01 mol dm^{-3} NaCl solutions were prepared and next to the pH was brought to a value between 3 and 10 by addition of 0.1 or 1 mol dm^{-3} HCl and 0.1 or 1 mol dm^{-3} NaOH. The samples of all studied carbon materials were added to solutions of appropriate pH and were shaken for 180 min at temperature 298°K. Then, the final pH was measured. The relationships between the final pH and the initial pH were constructed. The pH_{pzc} is the point where the line crosses, $pH_{initial} = pH_{final}$ [39,40]. The pH was measured with a pH-meter (inoLab pH 730 from WTW).

Table 1
The concentration of solutions used in the Boehm's method

Solution	Concentration (mol dm^{-3})	Functional groups
$NaHCO_3$	0.10	Carboxylic
Na_2CO_3	0.05	Carboxylic, lactone
NaOH	0.10	Carboxylic, lactone, phenolic
C_2H_5ONa	0.10	Carboxylic, lactone, phenolic, carbonyl
HCl	0.05	Total basic

2.4. Adsorption Experiments

In the experiments considering the pH effect, the solution pH values were adjusted from 2 to 10 by adding HCl (0.1 or 1 mol dm^{-3}) or NaOH (0.1 or 1 mol dm^{-3}) solutions.

Two synthesized carbon materials (with grain size from 0.2 to 0.8 mm) and commercial activated carbon were used for adsorption experiments. All adsorption experiments were carried out under the conditions presented in Table 2. Concentrations of orange II in solution before and after the adsorption were determined by the spectrophotometric method at a wavelength of 485 nm, using a spectrophotometer (SP-830 Plus from Metertech, Nangang, Taipei, Taiwan). Adsorption studies were carried out in 100 ml Erlenmeyer's flasks in an incubator (Orbital Shaker—Inkubator ES-20, Grant-bio) for defined time: sample weight 0.1 g, volume solution of OII 50 cm^3 (Table 2). The adsorption capacity of adsorbents for OII was designated by Eq. (1) [8]:

$$q_e - \frac{\left(C_0 - C_e\right)V}{m} \tag{1}$$

where q_e is the OII adsorption capacity (mg g^{-1}), C_0 is the initial concentration of OII solution (mg dm^{-3}); C_e is the concentration of OII solution after adsorption (mg dm^{-3}); V is the volume of the OII solution used for adsorption (dm^3); m is the adsorbent mass (g).

3. Results and discussion

3.1. Characterization of adsorbents

In Fig. 2, there are presented nitrogen adsorption isotherms (Fig. 2a) and pore size distributions (Fig. 2b) for studied adsorbents. According to International Union of Pure and Applied Chemistry classification [41] experimental isotherms (Fig. 2a) for the studied materials (ST-A and ST-A-CO_2) are

Table 2
The conditions of adsorption experiments for pH = 7

Experimental item	Studied carbon	OII solution concentration (mg dm^{-3})	Sampling time (min)	Temp. (K)	Vibration rate (rpm)
Adsorption isotherms	ST-A	100–1,200	600	298,308,315	200
	ST-A-CO_2	500–1,800	480	298,308,315	200
	CWZ-22	300–1,600	1,200	298,308,315	200
Adsorption kinetics	ST-A	100	30–1,440	298,308,315	200
	ST-A-CO_2	600	30–1,440	298,308,315	200
	CWZ-22	200	60–1,440	298,308,315	200

type IV, which are characteristic for mesoporous solids. The presence of accessible mesopores is confirmed by the H1 hysteresis loops. Isotherm for the CWZ-22 carbon is type I [41] which refers to adsorbents with the highly developed microporosity. In the range of low relative pressure, there is high nitrogen adsorption but in the area of medium and high relative pressures, the isotherm for CWZ-22 carbon has a course almost parallel to the abscissae axis, which indicates that mesoporosity (pores with dimensions of 2–50 nm) is poorly developed [42]. The type H4 hysteresis loop for CWZ-22 carbon is associated with narrow slit pores.

Structural parameters designated from adsorption isotherms are presented in Table 3. Investigated adsorbents have specific surface areas from 710 $m^2\ g^{-1}$ for carbon ST-A to 950 $m^2\ g^{-1}$ for carbon ST-A-CO_2. Achieved V_t values are from 0.43 $cm^3\ g^{-1}$ for carbon CWZ-22 to 0.85 $cm^3\ g^{-1}$ for carbon ST-A-CO_2. Micropores volumes V_{mi} are in the range from 0.22 $cm^3\ g^{-1}$ (ST-A) to 0.31 $cm^3\ g^{-1}$ (ST-A-CO_2 and CWZ-22). The mesoporosity (%) indicates that obtained in this work carbons (ST-A and ST-A-CO_2) contain primarily mesopores and commercial carbon is microporous. It should be underlined that the best parameters of the porous structure are found for the ST-A-CO_2, what should have a positive effect on the OII adsorption. This will be discussed in detail later in this work.

The distribution functions of pore volume (Fig. 2b) explicitly indicate that for the carbon CWZ-22 one pure peak was received in the range of micropores with maximum for w_{mi} = 0.73 nm, however for carbons synthesized in this work there are two peaks on the diagram, first in the micropores range and second in the mesopores range.

S_{BET}, BET specific surface area; V_t, total (single-point) pore volume obtained from the amount adsorbed at $p/p_0 \approx 0.99$; V_{ultra}, DFT volume of ultramicropores (pores < 0.7 nm) obtained on the basis of DFT PSD; V_{micro}, DFT volume of micropores (pores < 2 nm) obtained on the basis of DFT PSD; V_{meso}, DFT volume of mesopores (pores 2–50 nm) obtained on the basis of DFT PSD; w_{mi}/w_{me}, micropore/mesopore diameter at the maximum of the PSD curve obtained by the DFT method.

Figs. 3a and b present mesoporous structures of carbons ST-A. The visible channels are mesopores (in the majority), and micropores (in the minority). After CO_2 activation adsorbent structure has changed. A layered structure with marked mesopores channels is visible (Fig. 3c). The structure "similar to honeycomb" of this material can be observed (Fig. 3d). The CWZ-22 commercial carbon (Figs. 3e and f) presents a porous layered structure. There can be observed empty space in the majority of represented micropores and a much smaller number of mesopores.

The next stage in the analysis of adsorbent properties was the determination of surface functional groups containing oxygen and the pH_{PZC}. The marked functional groups on the surface of studied adsorbents are listed in Table 4. The prepared in this work carbons (ST-A and ST-A-CO_2) have more

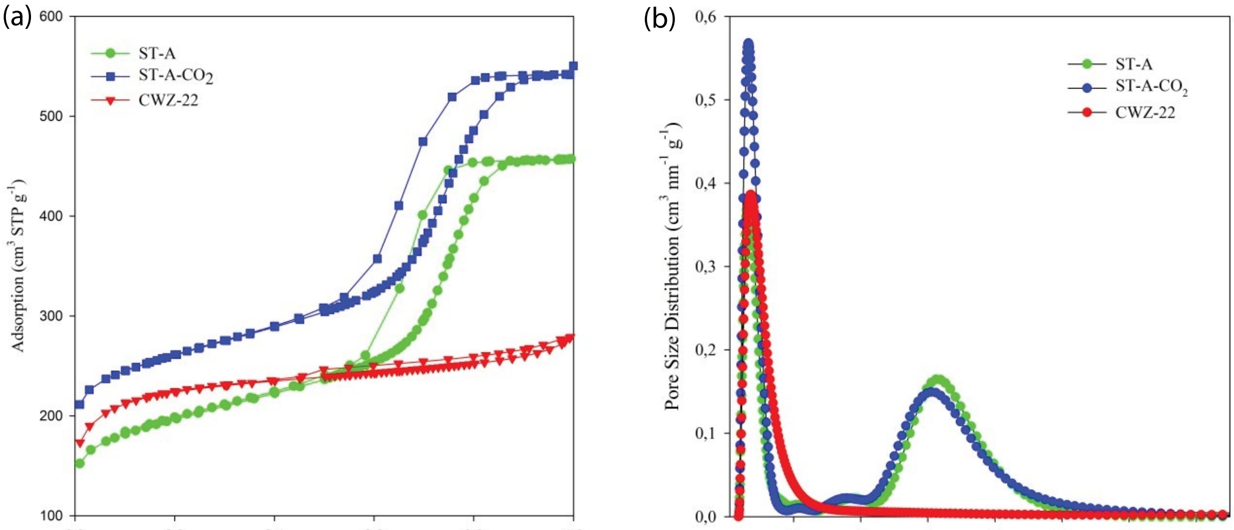

Fig. 2. Nitrogen adsorption isotherms (a) and pore size distribution (b) for studied carbon materials.

Table 3
Structural parameters of the studied adsorbents

Adsorbents	S_{BET} ($m^2\ g^{-1}$)	V_t ($cm^3\ g^{-1}$)	V_{ultra} ($cm^3\ g^{-1}$)	V_{micro} ($cm^3\ g^{-1}$)	V_{meso} ($cm^3\ g^{-1}$)	$w_{mi\ DFT}$ (nm)	$w_{me\ DFT}$ (nm)	Mesoporosity (%)
CWZ-22	775 [43]	0.43 [43]	0.08	0.31	0.12	0.73	–	28
ST-A	710	0.71	0.08	0.22	0.49	0.65	6.24	69
ST-A-CO_2	950	0.85	0.13	0.31	0.54	0.65	6.10	64

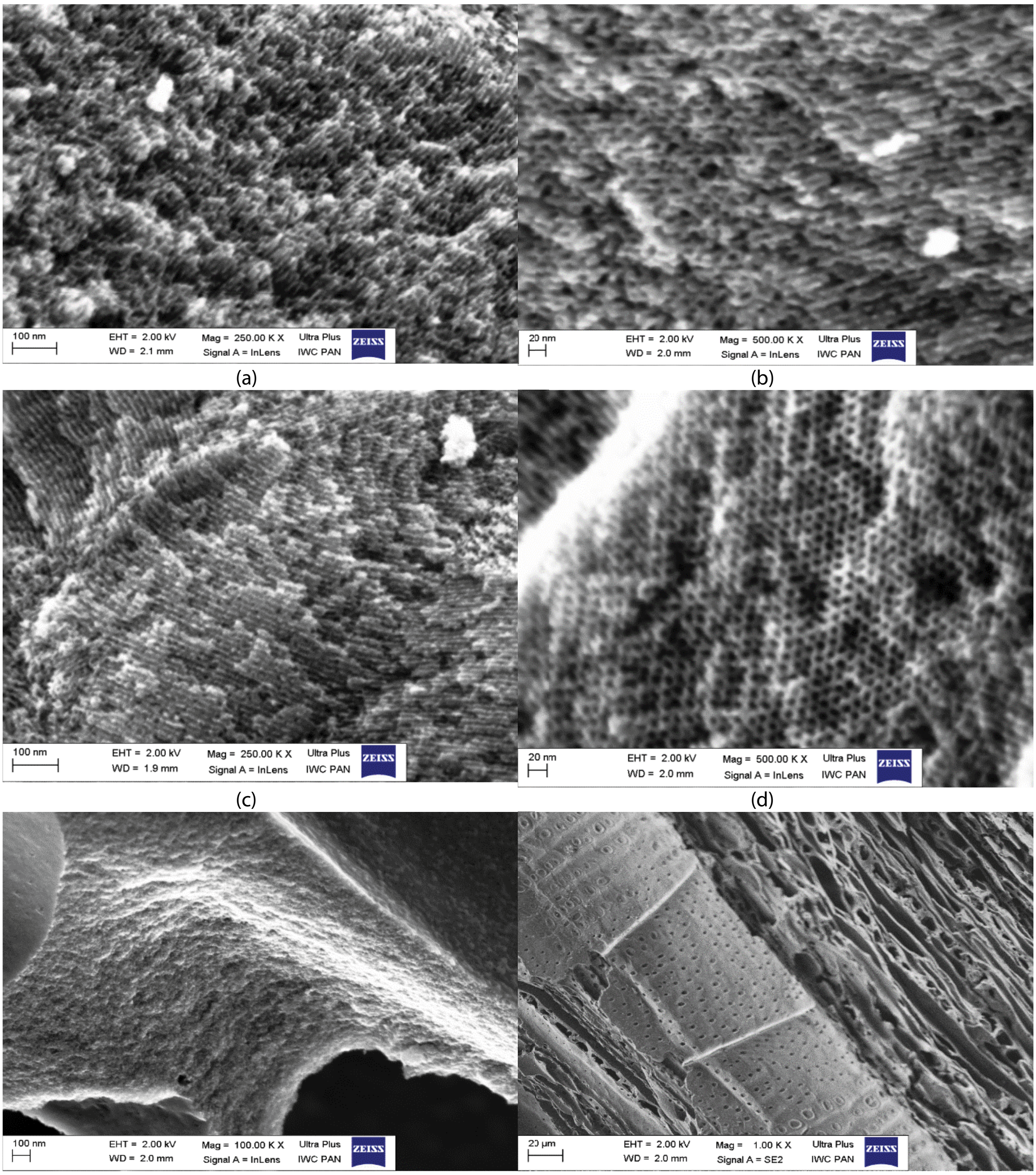

(a) (b)

(c) (d)

(e) (f)

Fig. 3. SEM images of samples: ST-A (a and b), ST-A-CO_2 (c and d), and CWZ-22 (e and f).

acidic properties, and the commercial carbon (CWZ-22), on the contrary, has more basic properties.

The pH_{pzc} determines the pH value at which the net surface charge on the adsorbent equals zero [39,44]. Fig. 4 presents the pH drift data method for studied carbons. The values pH_{pzc} are equal 8.06, 7.73, and 10.9 for ST-A, ST-A-CO_2, and CWZ-22, respectively. In solution of $pH < pH_{pzc}$ the carbon surface has a positive charge, while for $pH > pH_{pzc}$ the surface has a negative charge [39,44].

3.2. Adsorption properties

3.2.1. Effect of pH solution

Considering the efficiency of the adsorption process the pH should be taken into account, because it has got an essential influence on the charge aggregated on the adsorbent surface and it differentiates forms of adsorbate—orange II (Fig. 5) [45,46].

As it can be seen in Fig. 5. OII, in order of pH of the environment, may appear in the solution in a doubly protonated form (H_2L), single protonated form (HL^-), and unprotonated (L^{2-}).

Additionally, single protonated form of OII (HL^-) appears in two forms of tautomeric varieties. One of them is azo-enolic (azo tautomer) and the second hydrazine-ketonic form (hydrazine tautomer). In the solution, the equilibrium is shifted toward the azo tautomer. In a strongly acidic environment ($1 < pH > 2$) there are two forms side by side: H_2L and HL^- with the dominant participation of HL^- form. In the pH range from 2 to 9.6, there is only one form dominating HL^-. In the solutions with pH range from 9.6 to 10.6 there are HL^- and L^{2-} forms side by side, with domination of HL^- form, however for pH from 10.6 to 11.6 the dominating is unprotonated form (L^{2-}). In the solutions with pH higher than 11.6, only unprotonated form (L^{2-}) appears [45,46].

Fig. 6 shows the efficiency of dye removal from solutions in the range of pH of 2–10 on the tested adsorbents.

The value of pH_{PZC} for synthesized carbons ST-A and ST-A-CO_2 are 8.06 and 7.73, respectively, however for commercial carbon CWZ22 pH_{PZC} = 10.9 (Fig. 4). It can indicate that in the solutions with pH value $pH < pH_{PZC}$ on the surface of the adsorbent aggregates a positive charge. For all studied adsorbents, the greatest efficiency of the removal of dye was observed for solutions with pH = 2 (84% ST-A-CO_2, 80% ST-A, 65 % CWZ22; Fig. 6.). At such pH of the solution, the dye is present in H_2L and HL^- form (Fig. 5). Therefore the efficiency of the adsorption is related to electrostatic influence between the positive charge of the adsorbent surface and negative molecule of dye. From the pH = 3 the adsorption decreases and it remains practically at the same level till pH = 10. The amount of dye removed from the solution decreases to 63% for ST-A-CO_2, 55% for ST-A, and 49 % for CWZ-22 (Fig. 6.). The highest reduction of the sorptive capacity appears for

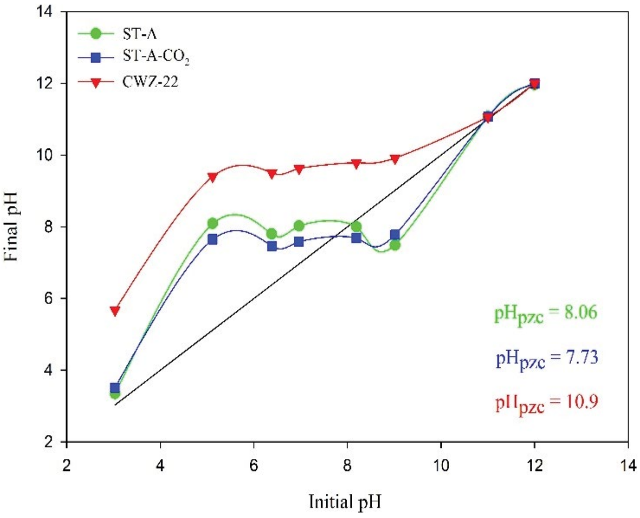

Fig. 4. The pH_{pzc} of studied adsorbents designated by the pH drift method.

Table 4
Oxygen functional groups on the surface of studied carbons

Adsorbents	Total basic groups (mmol g^{-1})	Total acidic groups (mmol g^{-1})	Phenolic groups (mmol g^{-1})	Lactone groups (mmol g^{-1})	Carboxylic groups (mmol g^{-1})	Carbonyl groups (mmol g^{-1})
ST-A	0.30	0.72	0.37	not determined	not determined	0.35
ST-A-CO_2	0.56	0.82	0.44	not determined	not determined	0.38
CWZ-22 [43]	0.85	0.36	not determined	not determined	not determined	0.36

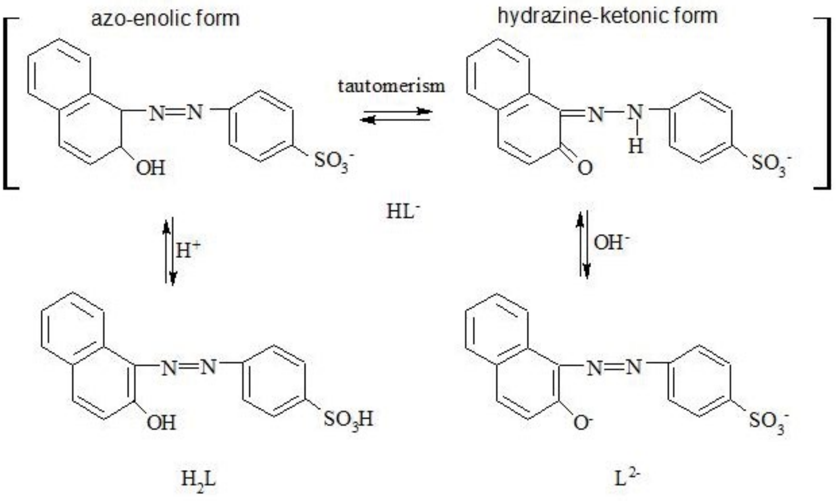

Fig. 5. The state changes of OII molecules with pH changes.

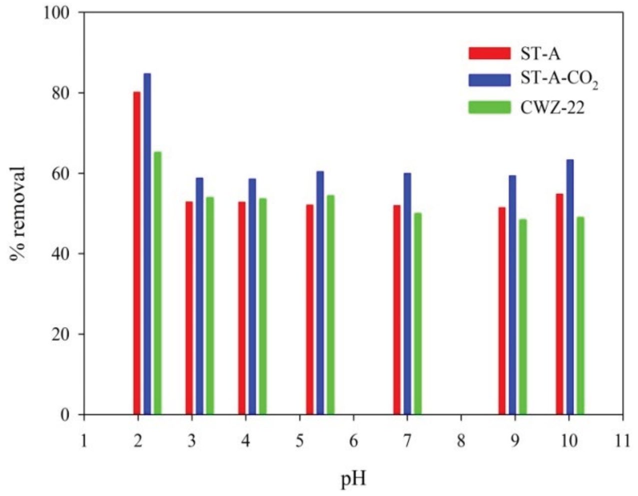

Fig. 6. Effect pH on the OII adsorption process for studied carbons.

material ST-A-CO$_2$ and the lowest for CWZ-22. Presented tendencies can be explained based on two factors: first with different values of pH$_{PZC}$ and various content of surface oxygen groups for investigated carbons. On the surface of synthesized carbons (ST-A and ST-A-CO$_2$) two acidic functional groups were present—hydroxyl (–OH) group and carbonyl (CO–) group, however on the surface of commercial carbon only the carbonyl group is present. The carbonyl group in an acidic environment is subjected to the transformation. As a result of the reaction, the adsorbent surface gains an additional positive charge, which is effective with the increase of electrostatic interaction between adsorbent and adsorbate.

Considering the presence of a phenolic group on the surface of the adsorbent it should be taken into account that in the alkaline environment this group is present as negative—phenolate. So in the alkaline environment, this group additionally increases the negative charge on the adsorbent surface. The result is the increased electrostatic repulsion between anion of the dye and a negative charge on the adsorbent surface. This effect can be observed most evidently

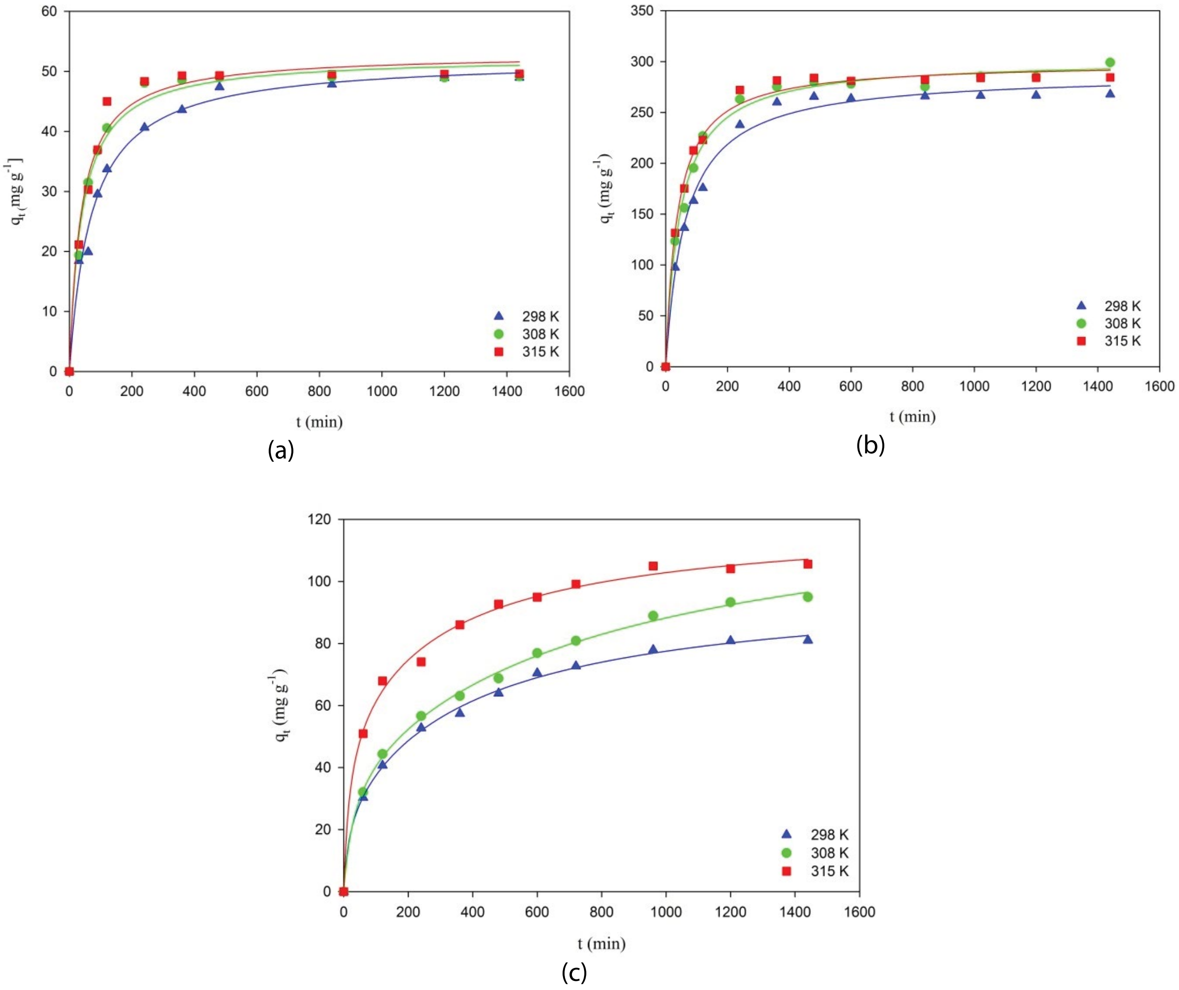

(a)

(b)

(c)

Fig. 7. Experimental kinetic adsorption curves (a–c) of orange II on studied carbon materials (ST-A, ST-A-CO$_2$, and CWZ-22, respectively).

for the carbon ST-A-CO$_2$, which contains the most phenolic groups on the surface. The significantly smaller degree of the efficiency of the adsorption can be observed for the commercial carbon without phenolic groups on the surface.

3.2.2. Adsorption Kinetics

The dependence of the adsorption magnitude from the time of the adsorption process is shown in Figs. 7a–c. From these figures indicate that initially over time the value of the adsorption changes violently for carbons synthesized (ST-A and ST-A-CO$_2$), however for commercial carbon becomes more gentle. The equilibrium state is reached most quickly for ST-A-CO$_2$ (480 min.), for ST-A after 600 min and for commercial carbon after 1,200 min.

To describe the OII adsorption kinetics from aqueous solutions on the studied carbon materials, a linear form of the pseudo-first-order model, called the Lagergren Eq. (2) [47], and a linear form of the pseudo-second-order model known also as Ho Eq. (3) [48] and Weber–Morris intra-particle diffusion model in Eq. (4) have been applied [49]:

$$\ln\left(q_e - q_t\right) = \ln q_e - k_1 t \tag{2}$$

$$\frac{t}{q_t} = \frac{1}{k_2 q_e^2} + \frac{t}{q_e} \tag{3}$$

$$q_t = k_{\mathrm{id}} t^{\frac{1}{2}} + c \tag{4}$$

where k_1, pseudo-first-order rate constants (min^{-1}); k_2, pseudo-second-order rate constants (g mg^{-1} min^{-1}); t, time of contact between the adsorbent and adsorbate (min); q_e, adsorption value after the equilibrium stabilization (mg g^{-1}); q_t, adsorption value in given time t (mg g^{-1}), respectively; k_{id}, intra-particle diffusion rate constant (mg g^{-1} min$^{-1/2}$); and c, intercept, which represents the thickness of the boundary layer (mg g^{-1}).

Figs. 8a–f show linear relationships resulting from the presented pseudo-first-order [Eq. (2)] and pseudo-second-order kinetic models [Eq. (3)]. Table 5 presents the kinetic parameters calculated for the OII adsorption rate on all carbons. Based on these results, it can be concluded that OII adsorption on the studied carbons can be described by a pseudo-second-order kinetic equation, which is additionally confirmed by high values of correlation coefficients (R^2 > 0.98). The rate of constants pseudo-second-order reactions increases with temperature ranging.

Considering the kinetics of the adsorption process from solution on the surface of porous solid it should be taken into account what is the influence of diffusion on the rate of the entire process. In compliance with literature data [7,9,39,46] the diffusion process can be divided into the following stages:

- volume diffusion; mass transport, that is, adsorbate transport to the external surface of the adsorbent,
- diffusion in boundary layer of solid-solution; diffusion through boundary layer to the external surface of the adsorbent,
- diffusion in pores, that is, intra-particle diffusion or diffusion inside the pores and to the inner surface of the adsorbent,
- reaching the equilibrium state, where the rate of intra-particle diffusion decreases in order to low concentration of the adsorbate in the solution,
- adsorption or desorption on the inner surface of pores.

First four stages are so called diffusion stages, however, the last stage is related to adsorption itself. The first stage doesn't have an influence on the rate of the entire process, on the condition that during measurements intensive mixing is applied. It is said that diffusion through the boundary layer and intra-particle diffusion, as the slowest stages, might be the factors that determine the rate of the entire process.

In Figs. 9a–c the dependence q_t vs. $t^{1/2}$ is showed for studied in this work systems, in three temperatures. For all studied adsorbents diagrams consisting of two straight-line sections were obtained. The first part of the plots on the left side of each diagram is related to intra-particle diffusion. If this section doesn't go through the origin of the coordinate system, the intra-particle diffusion is not the only stage determining the rate of the entire process. In Table 6. determined from the diagram values of k_{id} are collected, for each adsorbent in three temperatures. Furthermore, c constant values (the cut with y-axis) were determined, which answers the terminal thickness of layer.

Obtained constants of diffusion rate (k_{id}), for synthesized carbons (ST-A and ST-A-CO$_2$), increase with the temperature rise. This effect is particularly visible for carbon ST-A-CO$_2$. The phenomenon of the growth of diffusion the rate, with the temperature rise, can be explained by the increase of the mobility and kinetic energy of the adsorbate molecules. In higher temperatures, the molecules of adsorbate can migrate deeper and faster inside (inner volume) the pores. This phenomenon can be a result of endothermicness of the adsorption process. Determined c values are positive (Table 6.) what permits to infer that the intra-particle diffusion is not the only stage determining the rate of the entire process.

3.2.3. Adsorption Isotherms

Experimental adsorption isotherms of orange II on studied carbons ST-A, ST-A-CO$_2$, and CWZ-22, obtained in 298 K are shown in Fig. 10.

The courses of the curves for three mentioned carbons are very similar. It begins from the rapid increase of the adsorption, then saturation of the adsorbents surface takes place. The highest adsorption capacity in relation to orange II has carbon ST-A-CO$_2$ ($q_{m\ \mathrm{exp}}$ = 322 mg g^{-1}). For adsorbents ST-A and CWZ-22 maximum adsorption is 127 and 206 mg g^{-1}, respectively.

Langmuir [50], Freundlich [51], Langmuir–Freundlich [52], and Dubinin–Radushkevich [53,54] models were applied to interpret experimental adsorption isotherms.

Langmuir isotherm parameters q_m and K_L were calculated on the basis of the following Eq. (5) [50]:

$$q_e = \frac{q_m K_L C_e}{1 + K_L C_e} \tag{5}$$

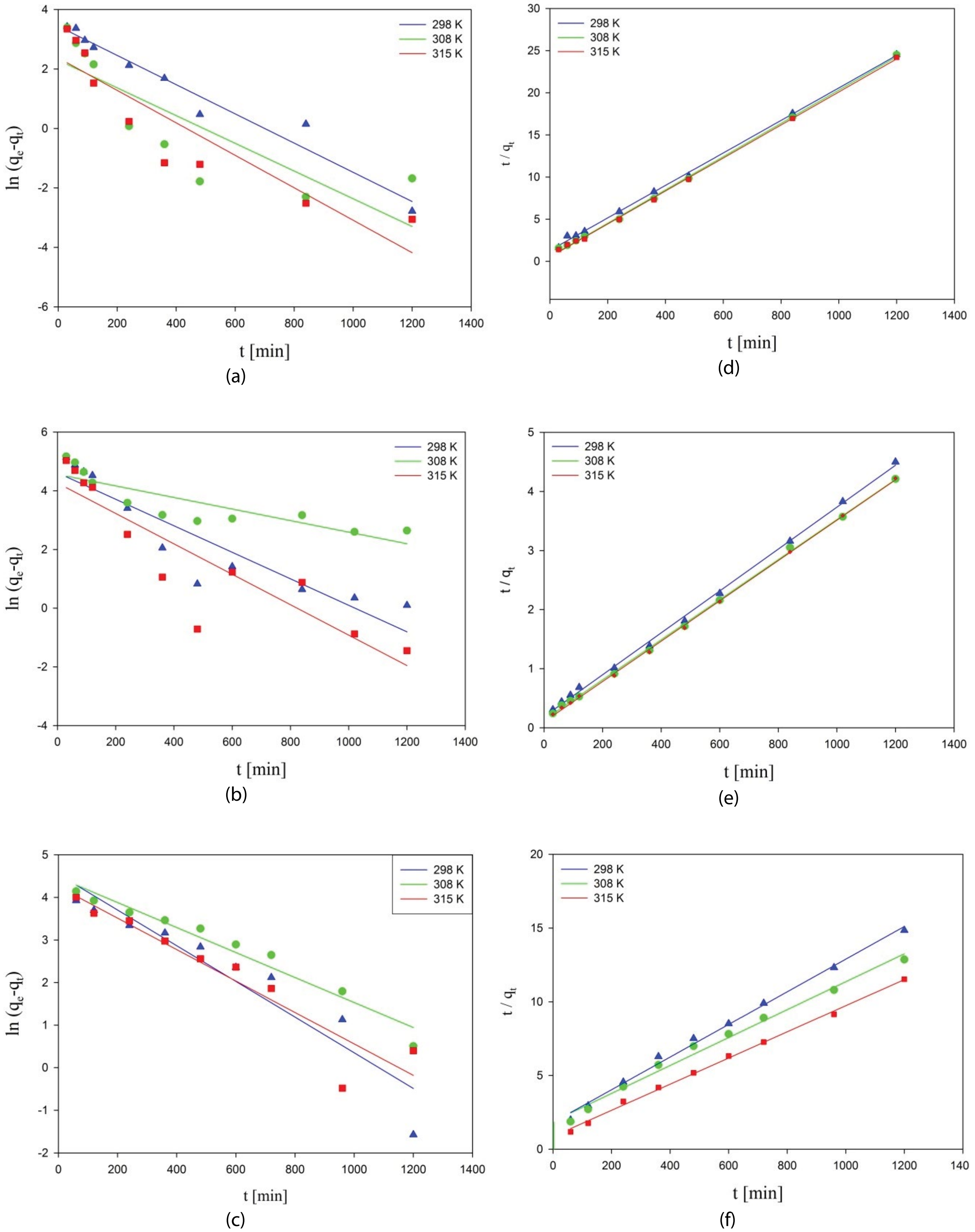

Fig. 8. Pseudo-first-order (a–c) and pseudo-second-order model (d–f) for ST-A, ST-A-CO_2, and CWZ-22, respectively.

Table 5
Kinetics parameters for the adsorption of OII on the tested adsorbents

Adsorbent	Temperature (°K)	Pseudo-first-order		Pseudo-second-order	
		k_1 (min^{-1})	R^2	k_2 (g mg^{-1} min^{-1})	R^2
ST-A	298	0.0049	0.9606	3.2×10^{-4}	0.9988
	308	0.0047	0.7028	7.2×10^{-4}	0.9991
	315	0.0055	0.8281	7.7×10^{-4}	0.9991
ST-A-CO$_2$	298	0.0045	0.8549	7.4×10^{-5}	0.9987
	308	0.002	0.7397	8.5×10^{-5}	0.9993
	315	0.0052	0.7993	1.2×10^{-4}	0.9995
CWZ-22	298	0.004	0.8955	6.8×10^{-5}	0.9948
	308	0.003	0.9574	4.8×10^{-5}	0.9888
	315	0.004	0.8907	9.2×10^{-5}	0.9976

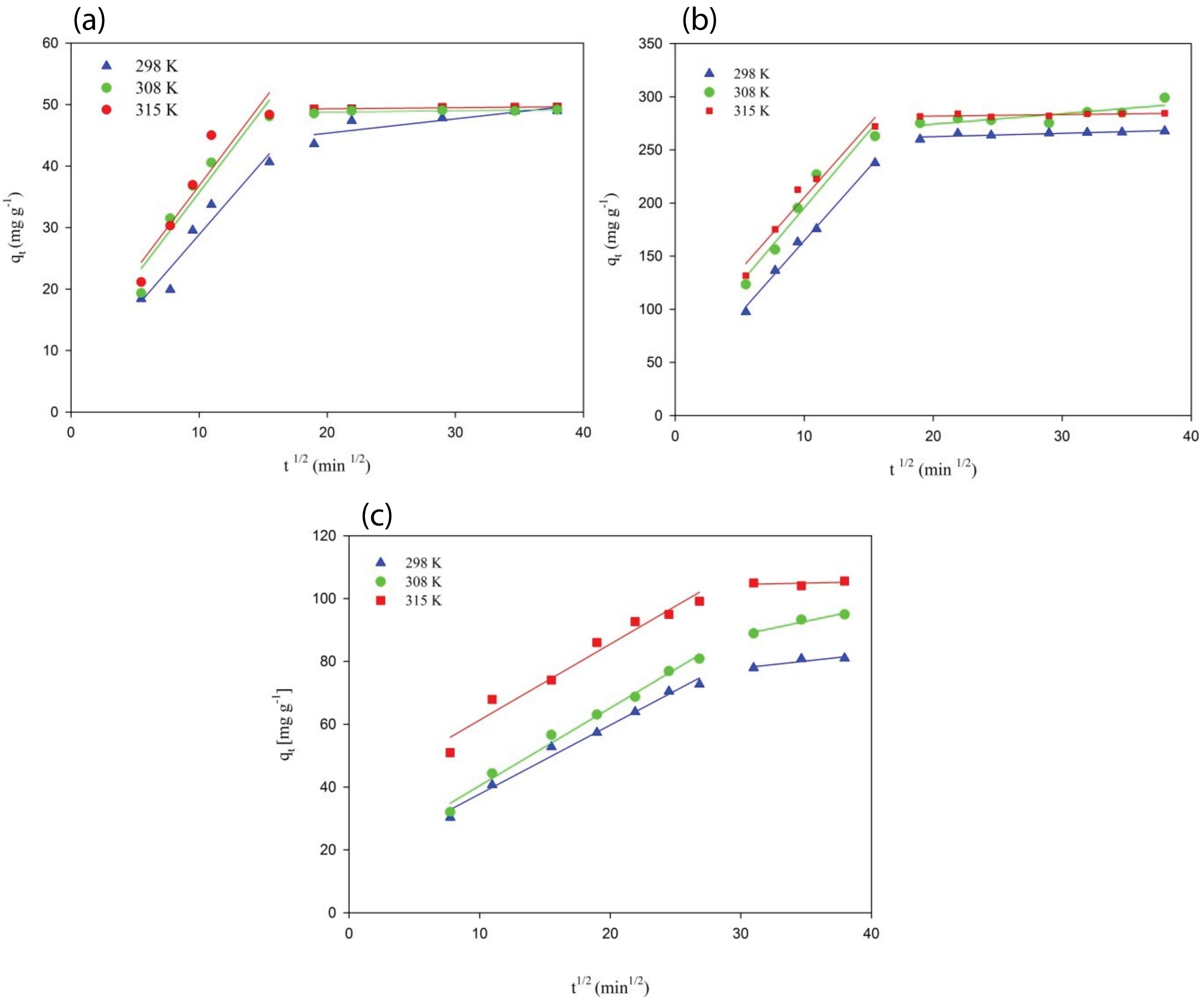

Fig. 9. The intra-particle diffusion (a–c) for ST-A, ST-A-CO$_2$, and CWZ-22, respectively.

Table 6
Intra-particle diffusion model parameters

Adsorbent	Temperature (°K)	k_{id} (mg g^{-1} min$^{-1/2}$)	c (mg g^{-1})	R^2
ST-A	298	2.39	4.88	0.9287
	308	2.74	8.34	0.9179
	315	2.75	9.26	0.8834
ST-A-CO_2	298	13.70	27.42	0.9931
	308	51.98	14.33	0.9514
	315	67.92	13.73	0.9604
CWZ-22	298	2.20	15.78	0.9860
	308	2.48	15.65	0.9889
	315	2.42	37.15	0.9620

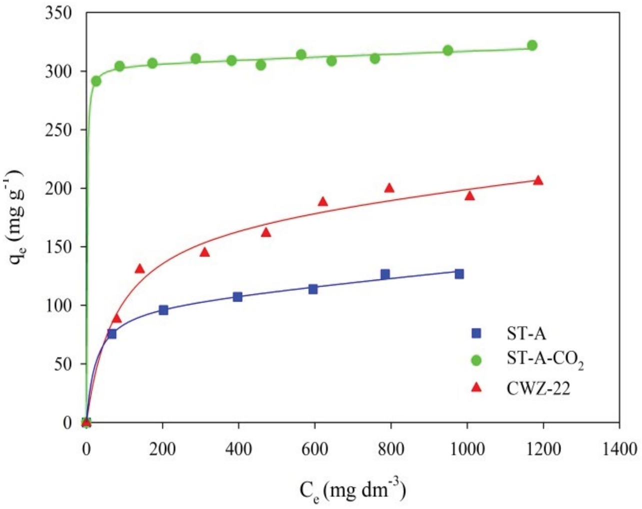

Fig. 10. Experimental adsorption isotherms of orange II on studied carbons.

where q_m is the maximum adsorption capacity corresponding to the total monolayer coverage on the adsorbent surface (mg g^{-1}); K_L is the Langmuir constant (dm^3 g^{-1}).

The relationship between experimental data q_e vs. C_e was additionally analyzed based on the Freundlich model [51]:

$$q_e = K_F C_e^{\frac{1}{n}} \tag{6}$$

where K_F is the Freundlich isotherm constant [mg$^{(1-1/n}$ (dm^3)$^{1/n}$ g^{-1}]; n is empirical constant describing the heterogeneity of the adsorbent surface.

The Langmuir–Freundlich (Sips) isotherm is presented in the form [52]:

$$q_m = \frac{q_m \left(K_{LF} C_e\right)^m}{1 + \left(K_{LF} C_e\right)^m} \tag{7}$$

where K_{LF} is the Langmuir–Freundlich constant (dm^3 mg^{-1}); m is constant.

The Dubinin–Radushkevich isotherm [53–55] describes adsorption in micropores, on homogeneous adsorbent surfaces.

$$q_e = q_m e^{-\beta\varepsilon^2} \tag{8}$$

$$\varepsilon = RT\left(\ln\left(1 + \frac{1}{C_e}\right)\right) \tag{9}$$

$$E = \frac{1}{\sqrt{2\beta}} \tag{10}$$

where ε is Polanyi potential; β is connected with adsorption energy (E) [Eq. (10)], which is defined as the free energy transfer of 1 mol of solute from the infinity of the surface of the sorbent.

The non-linear regression model using Origin Microcal 10 (together with the Levenberg-Marquardt algorithm) was applied in order to attribute an appropriate adsorption model and calculate adsorption parameters characteristic for each model.

The comparison of experimental values q_e vs. C_e with curves calculated on the basis of presented models is shown on diagrams in Figs. 11–13. On the basis of the graphic image of the discussed diagrams, it is very difficult to determine the appropriate model of adsorption, because the course of each diagram visually well-enrols to the experimental system of points. In the case of carbon ST-A-CO$_2$ curves, crossed out in compliance with equilibrium models of the Langmuir and Langmuir–Freunlich, adsorption overlap on themselves. The settlement of the problem of the proper model choice can be achieved parameters calculated in compliance with chosen theoretical equation parameters (Table 7) characterizing the adsorption process.

In the case of orange II adsorption on carbon, ST-A-CO$_2$ determined values of the exponent "m" in Langmuir–Freundlich equation are close to one, so this adsorption model turns to Langmuir equation.

From data are shown in Table 7. can be seen that in the case of two other carbon adsorbents, the proper model describing the adsorption process is also Langmuir isotherm.

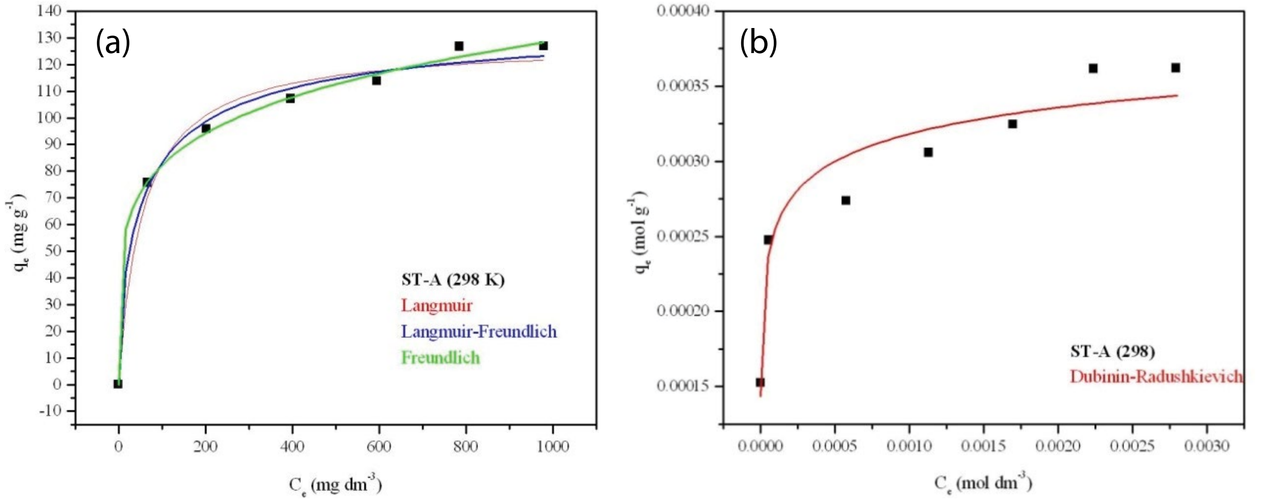

Fig. 11. (a) Langmuir, Langmuir–Freundlich, and Freundlich isotherms for ST-A in temp. 298°K and (b) Dubinin–Radushkevich isotherm for ST-A in temp. 298°K.

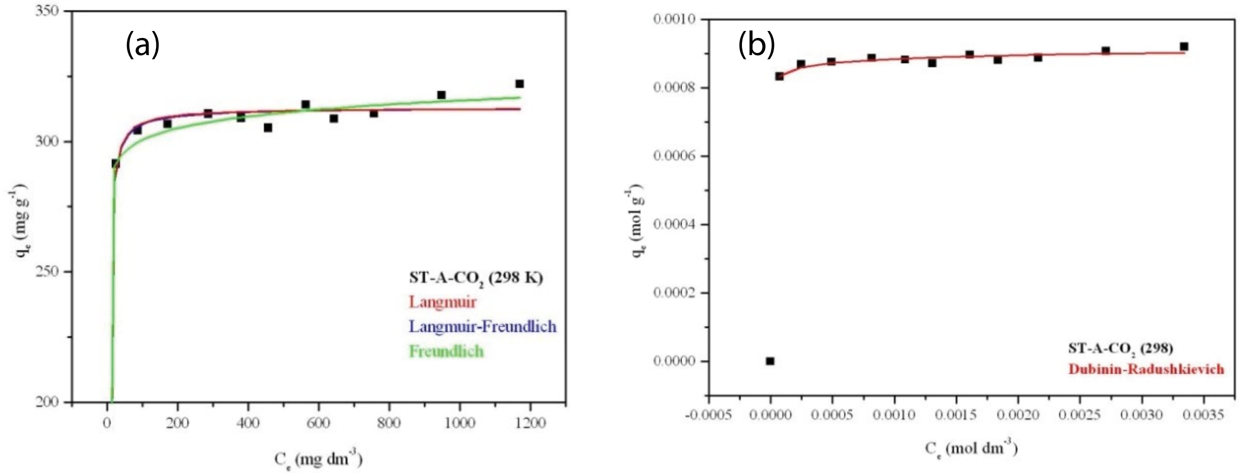

Fig. 12. (a) Langmuir, Langmuir–Freundlich, and Freundlich isotherms for ST-A-CO_2 in temp. 298°K and (b) Dubinin–Radushkevich isotherm for ST-A-CO_2 in temp. 298°K.

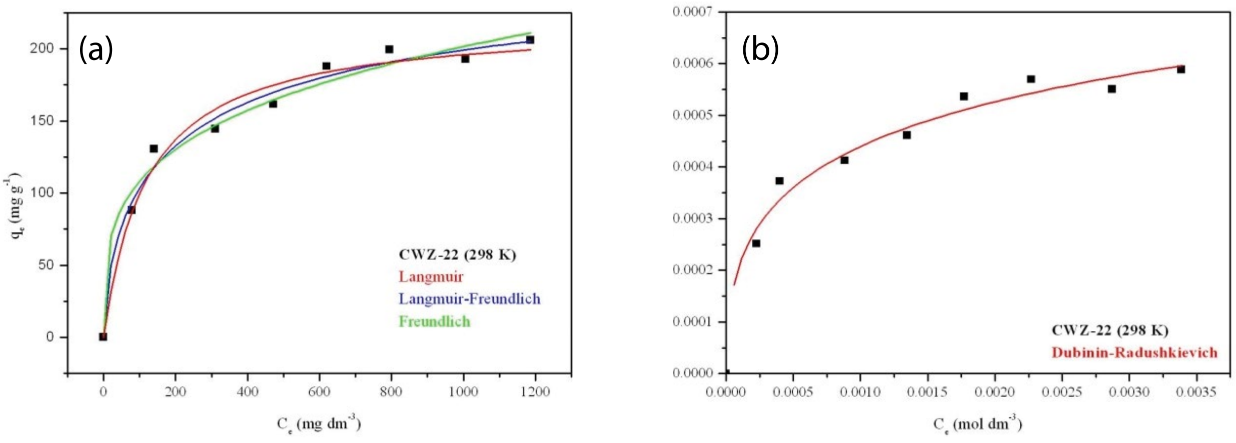

Fig. 13. (a) Langmuir, Langmuir–Freundlich, and Freundlich isotherms for CWZ-22 in temp. 298°K and (b) Dubinin–Radushkevich isotherm for CWZ-22 in temp. 298°K.

Table 7
Parameters from the Langmuir, Langmuir–Freundlich, Freundlich, and Dubinin–Radushkevich adsorption isotherm models

Carbon	Isotherm	Parameters	Temperature		
			298°K	308°K	315°K
ST-A	Langmuir	$q_{m\,\mathrm{exp}}$ (mg g$^{-1)}$	127	148	156
		q_m (mg g^{-1})	128	150	158
		K_L (dm^3 mg^{-1})	0.01824	0.02756	0.02933
		R^2	0.9856	0.9923	0.9969
	Langmuir–Freundlich	q_m (mg g^{-1})	142	158	154
		K_{LF} (dm^3 mg^{-1})	0.01692	0.01036	0.01998
		m	0.6795	1.25	1.439
		R^2	0.9870	0.9990	0.9972
	Freundlich	K_F [mg$^{1-1/n}$ (dm^3)$^{1/n}$ g^{-1}]	33.8	55.3	81.8
		n	5.16	6.85	10.76
		R^2	0.9977	0.9937	0.9942
	Dubinin–Radushkevich	q_m (mg g^{-1})	147	186	196
		β (mol^2 kJ^{-2})	9.62×10^{-10}	1.054×10^{-9}	1.02×10^{-9}
		E (kJ mol^{-1})	22.79	21.78	22.14
		R^2	0.933	0.922	0.943
ST-A-CO$_2$	Langmuir	$q_{e\,\mathrm{exp}}$ (mg g$^{-1)}$	322	346	359
		q_m (mg g^{-1})	313	332	340
		K_L (dm^3 mg^{-1})	0.4954	0.6475	0.7335
		R^2	0.9978	0.9894	0.9891
	Langmuir–Freundlich	q_m (mg g^{-1})	314	333	344
		K_{LF} (dm^3 mg^{-1})	0.69044	0.8267	1.0473
		m	0.8644	1.033	0.86
		R^2	0.9979	0.9907	0.9902
	Freundlich	K_F [mg$^{1-1/n}$ (dm^3)$^{1/n}$ g^{-1}]	273	290	281
		n	46.99	47.01	30.04
		R^2	0.9986	0.9964	0.9263
	Dubinin–Radushkevich	q_m (mg g^{-1})	329	368	378
		β (mol^2 kJ^{-2})	2.2×10^{-10}	3.49×10^{-10}	3.79×10^{-10}
		E (kJ mol^{-1})	47.67	37.85	36.32
		R^2	0.7104	0.899	0.843
CWZ-22	Langmuir	$q_{m\,\mathrm{exp}}$ (mg g^{-1})	206	226	268
		q_m (mg g^{-1})	219	235	266
		K_L (dm^3 mg^{-1})	0.0083	0.0125	0.0137
		R^2	0.9813	0.9809	0.9763
	Langmuir–Freundlich	q_m (mg g^{-1})	282	245	294
		K_{LF}(dm^3 mg^{-1})	0.00415	0.01239	0.01214
		m	0.61836	0.79926	0.7070
		R^2	0.9861	0.9882	0.9897
	Freundlich	K_F [mg$^{1-1/n}$ (dm^3)$^{1/n}$ g^{-1}]	31	43	52
		n	3.70	4.16	4.25
		R^2	0.9814	0.9899	0.9977
	Dubinin–Radushkevich	q_m (mg g^{-1})	396	406	459
		β (mmol^2 kJ^{-2})	2.7×10^{-9}	2.79×10^{-9}	3.23×10^{-9}
		E (kJ mol^{-1})	13.61	13.39	12.44
		R^2	0.9531	0.9807	0.9940

The values of maximum adsorption capacity (q_m) and regular (with temperature rise) change of the equilibrium constants K_L are in agreement with experimental values ($q_{m\,\mathrm{exp}}$). Large difference between the calculated value of the maximum sorptive (q_m) capacity and with experimental data appear in case of the Dubinin–Radushkevich model, for that reason determined parameters of this equation cannot be used to the interpretation of the adsorption process of the orange II on studied carbon adsorbents.

The parameters determined using the Langmuir, Langmuir–Freundlich, Freundlich, and Dubinin–Radushkevich adsorption isotherm models are presented in Table 7.

The dependence of the orange II adsorption process from the temperature on carbons ST-A, ST-A-CO$_2$, and CWZ-22 is illustrated in Figs. 14a–c. In the case of three studied adsorbents, the adsorption increase with temperature rise, for example, for ST-A-CO$_2$ is changing from 322 mg/g in 298 K temp. to 359 mg/g in 315 K temp., so the adsorption can be characterized as the endothermic process.

3.3. Adsorption thermodynamics and isosteric heat of adsorption

Determined equilibrium constants of Langmuir adsorption (K_L) were used for calculation of the following functions describing thermodynamics of studied adsorption processes: free enthalpy (ΔG), enthalpy (ΔH), and entropy (ΔS) [13,56].

$$\Delta G = -RT \ln K_L \tag{11}$$

$$\ln K_L = -\frac{\Delta H}{R} \times \frac{1}{T} + \frac{\Delta S}{R} \tag{12}$$

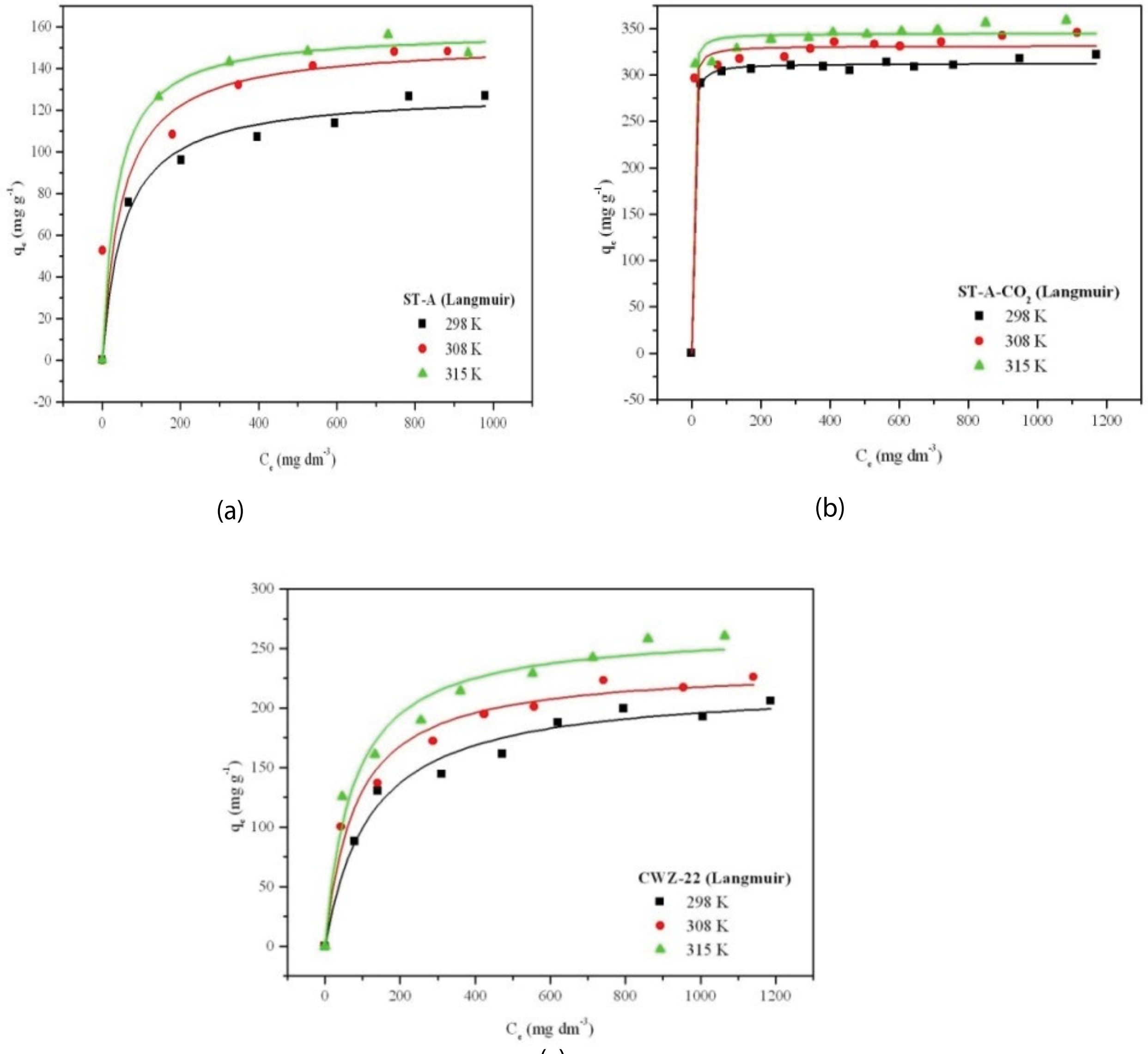

(a) (b)

(c)

Fig. 14. (a–c) Langmuir isoterms depending on the temperature for studied carbons.

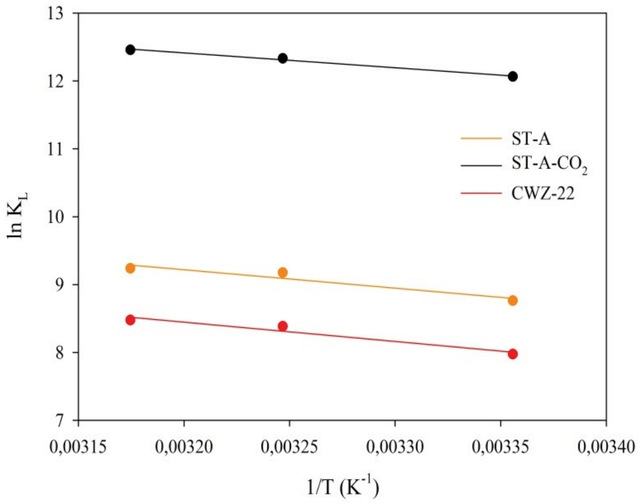

Fig. 15. Plot lnK_L = f(1/T) for all investigated adsorbents.

Table 9
Isosteric heat of orange II adsorption on studied carbons

Carbon	q_e (mg g^{-1})	ΔH_x (kJ mol^{-1})	R^2
ST-A	50	37.89	0.7264
	81	38.63	0.7277
	100	52.72	0.8959
ST-A-CO$_2$	302	74.63	0.8434
	309	105.47	0.9994
CWZ-22	71	39.00	1
	101	38.25	0.9999
	151	44.47	0.9999

Table 8
Thermodynamic parameters for OII adsorption on studied carbons

Carbon	T (K)	ΔG (kJ mol^{-1})	ΔH (kJ mol^{-1})	ΔS (J K^{-1} mol^{-1})
ST-A	298	–21.71	22.58	148.92
	308	–23.50		
	315	–24.20		
ST-A-CO$_2$	298	–29.90	18.21	161.48
	308	–31.58		
	315	–32.62		
CWZ-22	298	–19.76	23.67	145.97
	308	–21.47		
	315	–22.20		

Fig. 15. shows the dependence lnK_L = f(1/T). In Table 8. values of ΔG are collected, calculated from Eq. (11) and ΔH and ΔS values calculated from straight-line equation parameters, for example, 12, Fig. 15.

Obtained values of ΔG indicated that the adsorption process of OII is spontaneous in nature. Designated values of ΔH are positive which means, that the process is endothermic. The positive value ΔS indicates decrease in the randomness at the solid/solution interface during dye adsorption and provides information that the dye in the aqueous phase is in a more disordered distribution compared to the relatively ordered state of the solid phase (the surface of the adsorbent). The values of the determined parameters are similar to these obtained in the case of orange II adsorption studied on other carbon adsorbents. For example in work [57] for orange II adsorption process on AC-ZnO (AC = activated carbon), in temp. 288–318 K, the ΔG values are in the range from 1.626 to –4.372 kJ mol^{-1}, ΔH = 59.21 kJ mol^{-1}, ΔS = 199.95 J mol^{-1} K^{-1}. In another work [58] in the temperature range 293°K–303°K, the orange II adsorption on SBG adsorbent (spent brewery grains) is characterized by ΔG in range from –22.78 to –24.53 kJ mol^{-1}, ΔH = 28.66 kJ mol^{-1}, ΔS = 175.36 J mol^{-1} K^{-1}. The authors of work [63] studied the adsorption of orange II on AC (activated carbon) in temp. 293°K–313°K and obtained the following results: ΔG in range from –10.01 to –11.91 kJ mol^{-1}, ΔH = 17.85 kJ mol^{-1}, ΔS = 95.08 J mol^{-1} K^{-1}.

The isosteric heat of adsorption (ΔH_x) can be determined for individual values of the degree of surface. The value of isosteric adsorption heat is calculated on the basis of the Clausius–Clapeyron equation [56]:

$$\left(\frac{d\ln C_e}{dT}\right)_{q_e} = -\frac{\Delta H_x}{RT^2} \tag{13}$$

Its linear relationship is illustrated in the following Eq. (14):

$$\ln C_e = \frac{\Delta H_x}{R} \times \frac{1}{T} + \text{const} \tag{14}$$

To calculate the ΔH_x used in eg. 14. the received values ΔH_x are presented in the Table 9.

With the increase of surface coverage, the ΔH_x increases. This effect is the most evident for the ST-A-CO$_2$ carbon.

Table 10 compares the maximum adsorptive capasity (q_m) of studied in this work carbons with other types of adsorbents used for removal of OII. Our carbons are characterized by good properties in comparison to other adsorbents.

4. Conclusions

It was shown that mesoporous carbon material modified by carbon dioxide ST-A-CO$_2$, obtained in this work, is a proper adsorbent for OII dye removal from aqueous solutions. Unmodified mesoporous carbon ST-A and commercial CWZ-22 show lower adsorption properties in comparison to ST-A-CO$_2$. Material ST-A-CO$_2$ has the most developed porous structure from all adsorbents applied in this work, and it characterized by the presence of meso- and micro-pores.

Studying the influence of pH value on the adsorption process, pH$_{\text{PZC}}$ of analyzed carbons was considered and also the presence of surface functional groups containing oxygen determined by Boehm's method and dye form, which appears

Table 10
Comparison of the the maximum adsorptive capasity (q_m) of studied in this work carbons with other types of adsorbents

Adsorbent	pH	T (K)	q_m (mg/g)	References
ST-A	7	298–315	127–156	This study
ST-A-CO_2	7	298–315	322–359	This study
CWZ-22	7	298–315	206–268	This study
$CuFe_2O_4$/activated carbon[1]	5.2	298	392	[6]
Coconut powdered activated carbon	5.2	298	404	[6]
OBP[2]	6.3–6.9	298	25	[7]
BPAC[3]		298	333.33	[7]
Amberlite FPA-98[4]	7	298–323	100–200	[8]
SCG-GAC[5]	3	283–303	500–665.9	[9]
SBG[6]	4.5	293–303	28.54–30.47	[58]
Unmodified zeolite	1	298	0.63	[12]
Surfactant-modified zeolite	1	308	3.62	[12]
AC-ZnO[7]	3	288–318	19.68–60.55	[57]
ODTMA[8]	6.13	298	30.12–99.01	[59]
DODMA[9]	6.13	298	34.84–96.15	[59]
AC-SDVB[10]	7	298	625	[60]
OMC-PF[11]	7	298	108	[60]
AC-F400[12]	7	298	102	[60]
PAC[13]	2.8–10.5	298	400–440	[4]
GAC[14]: coconut shells	10	293	83.5	[61]
Almond nucleus	10	293	404.8	
Coal	10	293	170.7	
(AC) F-400[15]	3	303–338	384.3–698.5	[5]
AC[16]	7	293–313	147.09–389.02	[62]

[1]coconut powdered activated carbon, [2]original banana peel, [3]banana peel-activated carbon, [4]macroporous strongly basic anion exchange resin, [5]biomass-based granular activated carbon prepared by entrapping activated carbon powder derived from spent coffee grounds into calcium-alginate beads, [6]spent brewery grains, [7]activated carbon coated with zinc oxide, [9]Australian palygorskite modified with dioctadecyl dimethylammonium, [10]microporous carbon obtained from the polymer precursor—a sulphone-based styrene resin divinylbenzene, [11]mesoporous carbon material obtained from a phenol-formaldehyde resin by soft-templating method, [12]commercial carbon, Chemviron, England, [13]powdered activated carbon, [14]granular activated carbons, [15]activated carbon, Calgon, France, and [16]activated carbon was prepared from sawdust through co-calcinations with limestone.

for various pH values of the solution. It was shown that the highest percentage of dye removal took place in strongly acidic environment (pH = 2), where for the adsorption especially responsible is electrostatic interaction between the positive charge on the adsorbent surface (pH of the solution is lower than pH_{PZC}) and negative form of dye. The increase of the pH value up to 3 results in the decrease of adsorption properties. Additional increase of the pH from 3 to 10 doesn't change the adsorption properties which stay at the constant level.

The adsorption process kinetic can be described by pseudo-second-order equation. The constants rate of the process increase with temperature rise. It should be mentioned that the diffusion has an influence on the rate of the entire process, especially so called intra-particle diffusion.

Adsorption data were substituted into theoretical equations: Langmuir, Freundlich, Langmuir–Freundlich and Dubinin–Radushkevich. Applied mathematical models show that the adsorption process description is Langmuir equation.

The following thermodynamic functions of the adsorption process were calculated: free enthalpy ΔG, enthalpy ΔH, entropy ΔS, and ΔH_x. The process has spontaneous ($\Delta G < 0$) and endothermic ($\Delta H > 0$) character. The ΔS value is positive what indicates a decrease in randomness at the solid/solution interface during dye adsorption. The isosteric heat of adsorption (ΔH_x) increases with the increase of surface coverage.

Acknowledgments

This work was supported by Ministry of Science and Higher Education, Poland (research project 666 047).

References

[1] Z. Ezzeddine, I. Batonneau-Gener, Y. Pouilloux, H. Hamad, Removal of methylene blue by mesoporous CMK-3: Kinetics, isotherms and thermodynamics, J. Mol. Liq., 223 (2016) 763–770.

[2] L. Zhao, S.-T. Yang, S. Feng, Q. Ma, X. Peng, D. Wu, Preparation and application of carboxylated graphene oxide sponge in dye removal, Int. J. Environ. Res. Public Health, 14 (2017) 1301–1313.

[3] S. Hosseini, M.A. Khan, M.R. Malekbala, W. Cheah, T.S.Y. Choong, Carbon coated monolith, a mesoporous material for the removal of methyl orange from aqueous phase: adsorption and desorption studies, Chem. Eng. J., 171 (2011) 1124–1131.

[4] S. Aber, N. Daneshvar, S.M. Soroureddin, A. Chabok, K. Asadpour-Zeynali, Study of acid orange 7 removal from aqueous solutions by powdered activated carbon and modeling of experimental results by artificial neural network, Desalination, 211 (2007) 87–95.

[5] A. Rodríguez, J. García, G. Ovejero, M. Mestanza, Adsorption of anionic and cationic dyes on activated carbon from aqueous solutions: equilibrium and kinetics, J. Hazard. Mater., 172 (2009) 1311–1320.

[6] G. Zhang, J. Qu, H. Liu, A.T. Cooper, R. Wu, $CuFe_2O_4$/activated carbon composite: a novel magnetic adsorbent for the removal of acid orange II and catalytic regeneration, Chemosphere, 68 (2007) 1058–1066.

[7] J. Ma, D. Huang, J. Zou, L. Li, Y. Kong, S. Komarneni, Adsorption of methylene blue and Orange II pollutants on activated carbon prepared from banana peel, J. Porous Mater., 22 (2015) 301–311.

[8] S. Akazdam, M. Chafi, W. Yassine, B. Gourich, Removal of Acid Orange 7 dye from aqueous solution using the exchange resin amberlite FPA-98 as an efficient adsorbent: kinetics, isotherms, and thermodynamics study, J. Mater. Environ. Sci., 8 (2017) 2993–3012.

[9] K.-W. Jung, B.H. Choi, M.-J. Hwang, T.-U. Jeong, K.-H. Ahn, Fabrication of granular activated carbons derived from spent coffee grounds by entrapment in calcium alginate beads for adsorption of acid orange 7 and methylene blue, Bioresour. Technol., 219 (2016) 185–195.

[10] M. Czubaszek, J. Choma, Kinetic studies of selected dye adsorption from aqueous solutions on nanoporous carbons obtained from polymeric precursors, Ochr. Sr., 38 (2016) 3–12 (in Polish).

[11] S. Chen, M. Zhou, H.-F. Wang, T. Wang, X.-S. Wang, H.-B. Hou, B.-Y. Song, Adsorption of reactive brilliant red X-3B in aqueous solutions on clay–biochar composites from bagasse and natural attapulgite, Water, 10 (2018) 703–718.

[12] X. Jin, M. Jiang, X. Shan, Z. Pei, Z. Chena, Adsorption of methylene blue and orange II onto unmodified and surfactant-modified zeolite, J. Colloid Interface Sci., 328 (2008) 243–247.

[13] L. Yu, Y. Luo, The adsorption mechanism of anionic and cationic dyes by Jerusalem artichoke stalk-based mesoporous activated carbon, J. Environ. Chem. Eng., 2 (2014) 220–229.

[14] N. Mohammadi, H. Khani, V.K. Gupta, E. Amereh, S. Agarwal, Adsorption process of methyl orange dye onto mesoporous carbon material-kinetic and thermodynamic studies, J. Colloid Interface Sci., 362 (2011) 457–462.

[15] R. Ryoo, S.H. Joo, M. Kruk, M. Jaroniec, Ordered mesoporous carbons, Adv. Mater., 13 (2001) 677–781.

[16] A.H. Lu, W. Schmidt, B. Spliethoff, F. Schüth, Synthesis of ordered mesoporous carbon with bimodal pore system and high pore volume, Adv. Mater., 15 (2003) 1602–1606.

[17] J. Choma, Micro-mesoporous carbons: synthesis, properties, application, Inż. Ochr. Sr., 16 (2013) 163–178 (in Polish).

[18] R. Ryoo, S.H. Joo, S. Jun, Synthesis of highly ordered carbon molecular sieves via template-mediated structural transformation, J. Phys. Chem. B, 103 (1999) 7743–7746.

[19] J. Lee, J. Kim, T. Hyeon, Recent progress in the synthesis of porous carbon materials, Adv. Mater., 18 (2006) 2073–2094.

[20] T. Kyotani, Control of porous structure in carbon, Carbon, 38 (2000) 269–286.

[21] S. Jun, S.H. Joo, R. Ryoo, M. Kruk, M. Jaroniec, Z. Liu, T. Oshuna, O. Terasaki, Synthesis of new, nanoporous carbon with hexagonally ordered mesostructure, J. Am. Chem. Soc., 122 (2000) 10712–10713.

[22] S. Inagaki, K. Oikawa, Y. Kubota, Effect of carbon source on the textural and electrochemical properties of novel cage-type mesoporous carbon as a replica of KIT-5 mesoporous silica, Chem. Lett., 38 (2009) 918–919.

[23] C. Liang, K. Hong, G.A. Guiochon, J.W. Mays, S. Dai, Synthesis of a large-scale highly ordered porous carbon film by self-assembly of block copolymers, Angew. Chem. Int. Ed., 3 (2004) 5785–5789.

[24] S. Tanaka, N. Nishiyama, Y. Egashira, K. Ueyama, Synthesis of ordered mesoporous carbons with channel structure from an organic-organic nanocomposite, Chem. Commun., 16 (2005) 2125–2127.

[25] F. Zhang, Y. Meng, D. Gu, Y. Yan, C. Yu, B. Tu, D. Zhao, A facile aqueous route to synthesize highly ordered mesoporous polymers and carbon frameworks with Ia3d bicontinuous cubic structure, J. Am. Chem. Soc., 127 (2005) 13508–13509.

[26] J. Górka, A. Zawiślak, J. Choma, M. Jaroniec, KOH activation of mesoporous carbons obtained by soft-templating, Carbon, 46 (2008) 1159–1161.

[27] J. Jin, N. Nishiyama, Y. Egashira, K. Ueyama, Pore structure and pore size controls of ordered mesoporous carbons prepared from resorcinol/formaldehyde/triblock polymers, Microporous Mesoporous Mater., 118 (2009) 218–223.

[28] J. Choma, K. Jedynak, D. Jamioła, M. Jaroniec, Influence of carbonization temperature on the adsorption and structural properties of mesoporous carbons obtained by soft templating, Ochr. Sr., 34 (2012) 3–8 (in Polish).

[29] J. Choma, K. Jedynak, W. Fahrenholz, J. Ludwinowicz, M. Jaroniec, Development of microporosity in mesoporous carbons, Ochr. Sr., 35 (2013) 3–10 (in Polish).

[30] X. Wang, C.D. Liang, S. Dai, Facile synthesis of ordered mesoporous carbons with high thermal stability by self-assembly of resorcinol−formaldehyde and block copolymers under highly acidic conditions, Langmiur, 24 (2008) 7500–7505.

[31] J. Choma, A. Kalinowska, K. Jedynak, M. Jaroniec, Reproducibility of the synthesis and adsorption properties of ordered mesoporous carbons obtained by the soft-templating method, Ochr. Sr., 34 (2012) 1–8 (in Polish).

[32] N.P. Wickramaratne, M. Jaroniec, Activated carbon spheres for CO_2 adsorption, ACS Appl. Mater. Interfaces, 5 (2013) 1849–1855.

[33] S. Brunauer, P.H. Emmett, E. Teller, Adsorption of gases in multimolecular layers, J. Am. Chem. Soc., 60 (1938) 309–319.

[34] S.J. Gregg, K.S.W. Sing, Adsorption, surface area and porosity, 2nd ed., Academic Press, London, 1982.

[35] J. Jagiello, J.P. Olivier, 2D-NLDFT Adsorption models for carbon slit-shaped pores with surface energetical heterogeneity and geometrical corrugation, Carbon, 55 (2013) 70–80.

[36] J. Jagiello, J.P. Olivier, Carbon slit pore model incorporating surface energetical heterogeneity and geometrical corrugation, Adsorption, 19 (2013) 777–783.

[37] H.P. Boehm, Some aspects of the surface chemistry of carbon blacks and other carbons, Carbon, 32 (1994) 759–769.

[38] H.P. Boehm, Surface oxides on carbon and their analysis: a critical assessment, Carbon, 40 (2002) 145–149.

[39] C.K. Lim, H.H. Bay, C.H. Noeh, A. Aris, Z.A. Majid, Z. Ibrahim, Application of zeolite-activated carbon macrocomposite for the adsorption of Acid Orange 7: isotherm. kinetic and thermodynamic studies, Environ. Sci. Pollut. Res., 20 (2013) 7243–7255.

[40] J. Rivera-Utrilla, I. Bautista-Toledo, M.A. Ferro-García, C. Moreno-Castilla, Activated carbon surface modifications by adsorption of bacteria and their effect on aqueous lead adsorption, J. Chem. Technol. Biotechnol., 76 (2001) 1209–1215.

[41] K.S.W. Sing, D.H. Everett, R.A.W. Haul, L. Moscou, R.A. Pierotti, J. Rouquerol, T. Siemieniewska, Reporting physisorption data for gas/solid systems with special reference to the determination of surface area and porosity, Pure Appl. Chem., 57 (1985) 603–619.

[42] J. Choma, Characterization of nanoporous active carbons by using gas adsorption isotherms, Wegiel aktywny w ochronie srodowiska i przemysle, 2006, pp. 9–19 (in Polish).

[43] K. Jedynak, D. Wideł, N. Rędzia, Removal of Rhodamine B (a basic dye) and Acid Yellow 17 (an acidic dye) from aqueous solutions by ordered mesoporous carbon and commercial activated carbon, Colloids Interfaces, 3, (2019) 30–46.

[44] Y.S., Al-Degs, M.I. El-Barghouthi, A.H. El-Sheikh, G.M. Walker, Effect of solution pH, ionic strength, and temperature on adsorption behavior of reactive dyes on activated carbon, Dyes Pigm., 77 (2008) 16–23.

[45] C. Yin, C. Xu, W. Yu, Y. Jia, W. Sun, G. Zhou, M. Xian, Synthesis of a novel isatin and ethylenediamine modified resin and effective adsorption behavior towards Orange G, RSC Adv., 9 (2019) 801–809.

[46] L. Abramian, H. El-Rassy, Adsorption kinetics and thermodynamics of azo-dye Orange II onto highlyporous titania aerogel, Chem. Eng. J., 150 (2009) 403–410.

[47] S. Lagergren, About the theory of so-called adsorption of soluble substances, Kungl. Sven. Veten. Akad. Handl., 24 (1898) 1–39.

[48] Y.S. Ho, G. McKay, Pseudo-second-order model for sorption processes, Process Biochem., 34 (1999) 451–465.

[49] W.J. Weber, J.C. Morris, Kinetics of adsorption on carbon solution, J. Sanit. Eng. Div. Am. Soc. Civ. Eng., 89 (1963) 31–59.

[50] I. Langmuir, The constitution and fundamental properties of solids and liquids. Part I. Solids, J. Am. Chem. Soc., 38 (1916) 2221–2295.

[51] H.M.F. Freundlich, Over the adsorption in solution, J. Phys. Chem., 57 (1906) 385–470.

[52] J. Choma, M. Czubaszek, M. Jaroniec, Adsorption of dyes from aqueous solutions on active carbons, Ochr. Sr., 37 (2015) 3–14 (in Polish).

[53] M.M. Dubinin, L.V. Radushkevich, The equation of the characteristic curve of activated charcoal, Proc. Acad. Sci. USSR, 55 (1947) 331–337.

[54] M.M. Dubinin, The potential theory of adsorption of gasses and vapors for adsorbents with energetically nonuniform surfaces, Chem. Rev., 60 (1960) 235–266.

[55] S.M., Hasany, M.H., Chaudhary, Sorption potential of Hare River sand for the removal of antimony from acidic aqueous solution, Appl. Radiat. Isot., 47 (1996) 467–471.

[56] K. Kurdziel, M. Raczyńska-Żak, L. Dąbek, Equilibrium and kinetic studies on the process of removing chromium(VI) from solutions using HDTMA-modified halloysite, Desal. Water Treat., 137 (2019) 88–100.

[57] H. Nourmoradi, A.R. Ghiasvand, Z. Noorimotlagh, Removal of methylene blue and acid orange 7 from aqueous solutions by activated carbon coated with zinc oxide (ZnO) nanoparticles: equilibrium, kinetic, and thermodynamic study, Desal. Water Treat., 55 (2015) 252–262.

[58] J. Pedro Silva, S. Sousa, J. Rodrigues, H. Antunes, J.J. Porter, I. Gonçalves, S. Ferreira-Dias, Adsorption of acid orange 7 dye in aqueous solutions by spent brewery grains, Separ. Purif. Technol., 40 (2004) 309–315.

[59] B. Sarkar, Y. Xi, M. Megharaj, R. Naidu, Orange II adsorption on palygorskites modified with alkyl trimethylammonium and dialkyl dimethylammonium bromide - An isothermal and kinetic study, Appl. Clay Sci., 51 (2011) 370–374.

[60] M. Czubaszek, J. Choma, Adsorption of dyes from aqueous solutions on nanoporous carbon materials obtained from polymeric precursors, Ochr. Sr., 39 (2017) 3–10 (in Polish).

[61] X. Quan, X. Liu, L. Bo, S. Chen, Y. Zhao, X. Cui, Regeneration of acid orange 7-exhausted granular activated carbons with microwave irradiation, Water Res., 38 (2004) 4484–4490.

[62] L. Kong, M. Su, Y. Peng, L. Hou, J. Liu, H. Li, Z. Diao, K. Shih, Y. Xiong, D.Chen, Producing sawdust derived activated carbon by co-calcinations with limestone for enhanced Acid Orange II adsorption, J. Cleaner Prod., 168 (2017) 22–29.